Dynamic modeling and analysis of spacecraft with variable tilt of flexible appendages

Nicolas GUY
PhD Student
ONERA Centre de Toulouse
Systems Control and Flight Dynamics Dept.
31055 Toulouse, France
Email: nicolas.guy@onera.fr

Daniel ALAZARD
Professor
Université de Toulouse,DMIA,ISAE
31400 Toulouse, France
Email: daniel.alazard@isae.fr

Christelle CUMER[*†]
Researcher, at ONERA/Systems Control and Flight Dynamics Dept.
Email: christelle.cumer@onera.fr

Catherine CHARBONNEL
Research Engineer, at Thales Alenia Space
Email: catherine.charbonnel@thalesaleniaspace.com

ABSTRACT

This article describes a general framework to generate linearized models of satellites with large flexible appendages. The obtained model is parametrized according to the tilt of flexible appendages and can be used to validate an attitude control system over a complete revolution of the appendage. Uncertainties on the characteristic parameters of each substructure can be easily considered by the proposed generic and systematic multibody modeling technique, leading to a minimal LFT model. The uncertainty block has a direct link with the physical parameters avoiding non-physical parametric configurations. This approach is illustrated to analyze the attitude control system of a spacecraft fitted with a tiltable flexible solar panel. A very simple root locus allows the stability of the closed-loop system to be characterized for a complete revolution of the solar panel.

Nomenclature

As shown in Fig.1, this paper considers a satellite composed of a main rigid body $\mathcal{B}$ and only one appendage $\mathcal{A}$. Apart from the inertial frame $\mathcal{R}_o = (O, x_o, y_o, z_o)$ two other frames must be defined:

$\mathcal{R}_b = (B, x_b, y_b, z_b)$: main body reference frame also called "*rotating body frame*", where B is the center of mass of the main body

$\mathcal{R}_a = (P, x_a, y_a, z_a)$: appendage reference frame, where P denotes the anchorage point between the appendage and the main body

T_{ba} : transformation matrix from $\mathcal{R}_a$ to $\mathcal{R}_b$ defining the nominal configuration

Following notations will be used (vectors in a three-dimensional Euclidean space are indicated with an arrow, bold typeface is used for other vectors):

G_{total} : center of mass of the overall spacecraft

Concerning the main body $\mathcal{B}$:

$\overrightarrow{a}_B$: absolute linear acceleration vector of $\mathcal{B}$ at B
$\overrightarrow{a}_P$: absolute linear acceleration vector of $\mathcal{B}$ at P
$\overrightarrow{\omega}$: absolute angular velocity vector of $\mathcal{R}_b$ w.r.t $\mathcal{R}_o$
$\overrightarrow{F}_{ext}$: external forces vector applied to $\mathcal{B}$

$\overrightarrow{T}_{ext,B}$: external torques vector applied to $\mathcal{B}$ at B
$m^{\mathcal{B}}$: mass of the main body $\mathcal{B}$
$\mathbb{I}_B^{\mathcal{B}}$: 3×3 moment of inertia tensor of the main body $\mathcal{B}$ at B
τ_{PB} : kinematic model between the point P and the point B

Concerning the appendage $\mathcal{A}$:

G : center of mass of $\mathcal{A}$
$\overrightarrow{F}_{\mathcal{B}/\mathcal{A}}$: force vector applied by $\mathcal{B}$ to $\mathcal{A}$
$\overrightarrow{T}_{\mathcal{B}/\mathcal{A},P}$: torque vector applied by $\mathcal{B}$ to $\mathcal{A}$ at P
$\overrightarrow{T}_{\mathcal{B}/\mathcal{A},B}$: torque vector applied by $\mathcal{B}$ to $\mathcal{A}$ at B
$m^{\mathcal{A}}$: mass of the appendage $\mathcal{A}$
$\mathbb{I}_G^{\mathcal{A}}$: 3×3 moment of inertia tensor of the apenndage $\mathcal{A}$ at G

In case of a flexible appendage, some additional data must be defined:

N : number of flexible modes
$\boldsymbol{\eta}$: modal coordinates vector of flexible modes
ω_i : angular frequency of the i^{th} cantilevered flexible mode
ξ_i : damping factor of the i^{th} flexible mode
$\boldsymbol{l}_{i,P}$: 6×1 vector of participation factors of the i^{th} flexible mode computed at P
L_P : modal participation factor matrix computed at P

And finally, more general notations will be used:

s : LAPLACE variable
I_n : $n\times n$ identity matrix
$0_{n\times m}$: $n\times m$ zero matrix
A^T : A transposed
$\text{diag}(\omega_i)$: diagonal $N\times N$ matrix from ω_i, $i=1,\cdots,N$
$P(s)(i:j,l:m)$: subsystem of $P(s)$ between inputs l to m and outputs i to j
Acronyms
dof : degree of freedom
LFR : Linear Fractional Representation
LFT : Linear Fractional Transformation

1 Introduction

Future space missions have increasingly stringent requirements on pointing accuracy. Larger and more flexible satellite structures introduce flexible modes and challenge the limits of achievable pointing accuracy based on traditional AOCS (Attitude Orbit Control System) designs. The model of a flexible appendage (solar panel, antenna, ...), as derived by structural dynamics experts, assumes that the appendage is cantilevered at the anchorage point P and is given in terms of frequencies, dampings, and modal participation factors. The control design engineer has to gather the various appendage models on the main body model while taking the spacecraft geometry into account, in order to design and to validate the attitude control law. As he is involved very early in the project, the exact definition of the satellite is not yet fixed: that is the reason why many parameter values are supposed to be submitted to large uncertainties. Robust control design strategies are then preferred, requiring prior modeling of the feasible whole spacecraft set.

Currently the spacecraft dynamic model is written as a relationship between the 6 dof vector of the external forces and torques applied to the main body and the 6 dof vector of acceleration at the composite center of mass. Under small angles and angular rates assumption, a linearized model is commonly adopted to design attitude control laws. Some formulations are based on generalized damped spring/masses systems: they typically involve mass, damping and stiffness matrices of the coupled system [1–5]. In these formulations, the physical parameters of each substructure are cast in the whole model and the propagation of uncertainties cannot be derived easily. Furthermore, the dynamic model of the coupled system must be computed for a given angular configuration of appendages leading to high CPU-time for simulation and analysis of the coupled system over a complete revolution of appendages (typically a solar panel). Considering that the only external forces and torques applied on the appendage are the forces and torques applied by main body at the interface, other formulations exploit the multibody modeling approach and use directly the rough data of each substructure. Such an approach is helpful if substructures are designed and produced by different partners. Substructure couplings were first introduced in [6] through

the Component Mode Synthesis. Effective mass/inertia matrix [7] or impedance matrix [8] is quite convenient to build step-by-step the overall spacecraft model from subsystems, defined by their own physical and independent parameters [9].

If parametric uncertainties have to be taken into account in either of these two formulations, physical constraints must still be respected. Practically, the variations on the total mass/inertia of an appendage and the variations on its modal participation factors cannot be independent, otherwise some unrealistic parametric configurations may occur leading to unstable mechanical models [1, 10]. Mathematically, the residual mass matrix (defined as the difference between total mass of the appendage and effective masses of all flexible modes) of each appendage must be semi definite positive. In case of very flexible appendages this residual mass is in fact due to the contribution of neglected flexible modes (the residual mass tends to zero if all flexible modes are taken into account). As residual mass does not explicitly appear anywhere, it is difficult to introduce these inequality constraints into the LFT framework. The interest of substructure from the uncertainty modeling point of view is adressed in [11, 12] for robust control design purposes. In [11], the parametric uncertainty is focused on the interface stiffness. The substructure uncertainty is restricted to an unstructured uncertainty to handle high frequency truncated modes. In [12], the parametric uncertainty concerns only frequencies and damping ratios of each component mode. Uncertainty on mode shape (or effective mass) is not directly taken into account.

The first contribution of this paper is to propose a generic modeling approach for satellites with large flexible appendages for controller validation and simulation rather than for control design. The approach allows to take into account the substructure parametric uncertainty on mode frequencies, damping ratios and participation factors as they can be expressed by the substructure designers. This approach ensures to obtain a minimal realization of the satellite model and a minimal LFR-type representation of uncertainties, because it allows to come back to physical origins of the parameter variations. The second main contribution concerns the LFR of the appendage tilt angle, which offers an adequate framework to analyze the control law robustness for a complete revolution of each appendage.

The paper is organized as follows. Section 2 details the substructure approach used to build the linearized spacecraft model around a nominal configuration. When uncertainties are considered, the same handlings will be applied. However special attention is paid to the positiveness of appendage residual mass matrix, which has to be verified at each feasible parameter value. This leads to a new LFR formulation presented in section 3.1. Section 3.2 explains how parametrization of appendage tilt angle can be introduced into the new LFR formulation. The interest of this parametrization is then illustrated in section 4 through the validation of a control law robustness. Finally, section 5 concludes on remarks about the role of this new formulation and approach in flexible space structures control today.

2 Multibody modeling approach

Papers [1, 9, 10] propose various formulations to set up a linear dynamic model of a spacecraft with rigid or flexible appendages around a nominal configuration. The most commonly used formulation called "MDK" is based on data given by structural experts. Figure 2 represents such a formulation, where $\mathbb{M}$, $\mathbb{K}$ and $\mathbb{D}$ are respectively the generalized mass, stiffness and damping matrices of the whole spacecraft including rigid and flexible degrees of freedom. In [13], this formulation is cast into a left-coprime factorisation to handle uncertainty modeling for control design purpose with improved stability margins. Despite its simplicity, this formulation has two main drawbacks. Firstly this model is not appropriate to take physical uncertainties into account. Indeed, it is difficult to go back to the physical origin of these model parameter variations. Secondly the model must be recalculated for each angular configuration of the appendage.

The idea of the papers [9, 10] is to introduce a multibody modeling approach which splits the dynamic model of each body within the global system, before connecting them.

2.1 Main body model

The main body model is obtained thanks to EULER / NEWTON equations applied to the main body at point B (see the nomenclature). Under the small angular rate assumption (i.e. the CORIOLIS and centrifugal accelerations are neglected) and considering that the main body is rigid and submitted to external forces/moments $\overrightarrow{F}_{ext}$, $\overrightarrow{T}_{ext,B}$ and to forces/moments $\overrightarrow{F}_{\mathcal{B}/\mathcal{A}}$, $\overrightarrow{T}_{\mathcal{B}/\mathcal{A},P}$ due to the interaction with the appendage, this model reads:

$$\begin{bmatrix} \overrightarrow{F}_{ext} - \overrightarrow{F}_{\mathcal{B}/\mathcal{A}} \\ \overrightarrow{T}_{ext,B} - \overrightarrow{T}_{\mathcal{B}/\mathcal{A},B} \end{bmatrix} = D_B^{\mathcal{B}} \begin{bmatrix} \overrightarrow{a}_B \\ \dot{\overrightarrow{\omega}} \end{bmatrix}. \tag{1}$$

where:

$$D_B^{\mathcal{B}} = \begin{bmatrix} m^{\mathcal{B}} I_3 & 0_{3\times 3} \\ 0_{3\times 3} & \mathbb{I}_B^{\mathcal{B}} \end{bmatrix}. \tag{2}$$

2.2 Dynamic model of the cantilevered appendage

The dynamic model $M_P^{\mathcal{A}}(s)$ of the flexible appendage $\mathcal{A}$ cantilevered on the main body at the interface point P is commonly described by the so-called *Cantilever Hybrid Model* [1, 5, 9]. This model gives the relationship between the 6 dof acceleration vector of the point P, $\begin{bmatrix} \overrightarrow{a}_P \\ \overrightarrow{\dot{\omega}} \end{bmatrix}$, and the 6 dof forces/moments vector applied by main body to the appendage at point P, $\begin{bmatrix} \overrightarrow{F}_{\mathcal{B}/\mathcal{A}} \\ \overrightarrow{T}_{\mathcal{B}/\mathcal{A},P} \end{bmatrix}$:

$$\begin{cases} \begin{bmatrix} \overrightarrow{F}_{\mathcal{B}/\mathcal{A}} \\ \overrightarrow{T}_{\mathcal{B}/\mathcal{A},P} \end{bmatrix} = D_P^{\mathcal{A}} \begin{bmatrix} \overrightarrow{a}_P \\ \overrightarrow{\dot{\omega}} \end{bmatrix} + L_P \ddot{\boldsymbol{\eta}} \\ \ddot{\boldsymbol{\eta}} + diag(2\xi_i\omega_i)\dot{\boldsymbol{\eta}} + diag(\omega_i^2)\boldsymbol{\eta} = -L_P^T \begin{bmatrix} \overrightarrow{a}_P \\ \overrightarrow{\dot{\omega}} \end{bmatrix} \end{cases} \tag{3}$$

where:

- $D_P^{\mathcal{A}}$ is the 6×6 mass/inertia model matrix of the appendage at point P (see also appendix A),
- $L_p = [\boldsymbol{l}_{1,P}, \cdots, \boldsymbol{l}_{i,P}, \cdots, \boldsymbol{l}_{N,P}]$ is the matrix of modal participation factors of the N flexible modes of the appendage at point P,
- ω_i, ξ_i and $\boldsymbol{l}_{i,P}$ are the pulsation, the damping ratio and the 6 dof participation factor vector of the i-th flexible mode.

Equation (3) must be projected into the $\mathcal{R}_a$ frame. For equation legibility the projection frame is not mentionned.

All these data ($D_P^{\mathcal{A}}$, ω_i, ξ_i and $\boldsymbol{l}_{i,P}$) are directly provided by the finite element software used to model such an appendage according to the number N of flexible modes retained in the model and are independent of the main body characteristics.

Another well-known frequency-domain representation of $M_P^{\mathcal{A}}(s)$, also called effective mass/inertia model [7], can be easily derived from (3):

$$M_P^{\mathcal{A}}(s) = D_{P,0}^{\mathcal{A}} + \Sigma_{i=1}^{N} M_{i,P} \frac{2\xi_i\omega_i s + \omega_i^2}{s^2 + 2\xi_i\omega_i s + \omega_i^2} \tag{4}$$

where:

- $D_{P,0}^{\mathcal{A}} = D_P^{\mathcal{A}} - \Sigma_{i=1}^{N} M_{i,P} = D_P^{\mathcal{A}} - L_P L_P^T$ is the 6×6 residual mass/inertia of the appendage rigidly cantilevered to the main body at point P,
- $M_{i,P} = \boldsymbol{l}_{i,P}\boldsymbol{l}_{i,P}^T$ is the 6×6 effective mass/inertia matrix of the i-th flexible mode. $M_{i,P}$ is a rank-1, semi-definite positive matrix for all i.

The appendage dynamic model $M_P^{\mathcal{A}}(s)$ can also be represented by the block-diagram depicted in Fig. 3.

2.3 Connection of the main body and the flexible appendage

To connect the appendage model to the main body model, the Eqn. (3) must be moved from point P to point B (using the kinematic model τ_{BP}, see appendix A) and then must be written in $\mathcal{R}_b$ (using T_{ba}), before being insered into the Eqn. (1). The block diagram representation of the inverse dynamic model $[M_B^{\mathcal{A}+\mathcal{B}}(s)]^{-1}$ of the coupled system, presented in Fig. 4, shows that the direct appendage dynamic model $M_P^{\mathcal{A}}(s)$ at point P interacts as a feedback on the inverse main body dynamic model $\left[D_B^{\mathcal{B}}\right]^{-1}$. Consequently characteristic parameters of each body can be highlighted in such a block-diagram representation. This approach has the advantages

- to fit into the block-diagram as many (rigid or flexible) appendages as possible through other feedbacks on $\left[D_B^{\mathcal{B}}\right]^{-1}$,
- to minimize the number of occurrences of each physical parameters of each body,
- to directly access to them and finally to take easily into account their uncertainties.

Finally, the model of the satellite can be translated to the global center of mass:

$$M_{G_{total}}^{\mathcal{A}+\mathcal{B}}(s) = \tau_{BG_{total}}^T M_B^{\mathcal{A}+\mathcal{B}}(s) \tau_{BG_{total}} \ . \tag{5}$$

Regarding the design and the validatation of the attitude control system, the inverse dynamics model of the spacecraft is then restricted to the 3 angular dof and is completed by the double integrators between the angular acceleration $\overrightarrow{\dot{\omega}}$ and the 3 pointing error vector $\overrightarrow{\theta} = [\theta_x, \theta_y, \theta_z]^T$ of the main body (in the frame $\mathcal{R}_b$). This model is depicted in Fig. 5 and will be denoted $H(s)$ in the sequel.

3 Model with uncertain and varying parameters

The following two subsections consider respectively:

- the uncertainties on the main dynamic parameters of the main body and appendages: some recommendations for extracting the LFR of the uncertain model which is required to validate the attitude control system are given,
- the variation of the tilt angle of the appendage. Indeed, considering that the appendage is a sun-oriented solar pannel, the tilt angle describes a complete revolution over one orbital period. This motion is very slow and one can consider that the solar pannel is cantilevered on the main body with a varying tilt angle. This tilt angle has a direct influence on the dynamic behavior of the coupled system and the attitude control system must be robust to such a variation.

3.1 Parametric uncertainties modeling

The general LFT framework consists in isolating the uncertainty matrix Δ from the nominal system $H(s)$ and in connecting them through a feedback as represented in Fig. 6. It is commonly used as input for μ-analysis tools to perform robustness analysis [5,14]. For numerical reasons, a minimal LFR realization (in sense of a minimal size of Δ) is often searched [15,16]. Indeed the complexity of μ-analysis directly depends on this uncertainties block size. Appendix B illustrates with a simpler model the difficulty in obtaining numerically a minimal LFR. This academic example highlights why the minimal LFR of an uncertain model is not so obvious and must be tackled very soon in the modeling phase. Note that the block diagram description of the model presented in Fig. 3 and 4 is key to extract the global LFR. Each block (each parameter) can be viewed as an elementary LFR object and the minimal LFR of the overall spacecraft can be easily obtained using the LFRT toolbox [17]. The number of occurences of flexible mode parameters ω_i (2 times), ξ_i (1 times) and coefficients of matrix L_P (2 times each) is thus minimized.

Lastly, it is worth expressing appendage uncertainties on the parameters $D_{P,0}^{\mathcal{A}}$ and L_P rather than on the parameters $D_P^{\mathcal{A}}$ and L_P. The constraint on the positiveness of the residual mass:

$$D_{P,0}^{\mathcal{A}} = D_P^{\mathcal{A}} - L_P L_P^T \geq 0 \tag{6}$$

must be satisfied for any parametric configurations [1]. Indeed, as $D_{P,0}^{\mathcal{A}}$ acts in feedback on the inverse dynamics of the coupled system, a non-positive matrix could lead to unstable free flexible modes which is obviously physically impossible. The physical constraint (6) can be transgressed, when parametric uncertainties on both L_P and $D_P^{\mathcal{A}}$ are considered independently in equation (3).

3.2 LFR of the appendage with a varying tilt angle

This section considers the tilt of the cantilevered appendage around the y_a-axis according to Fig. 7. First of all, the appendage dynamic model $M_P^{\mathcal{A}}(s)$ must be replaced by $RM_P^{\mathcal{A}}(s)R^T$ in Fig. 4 where:

$$R = \begin{bmatrix} R_\alpha & 0_{3\times3} \\ 0_{3\times3} & R_\alpha \end{bmatrix} \text{ and } R_\alpha = \begin{bmatrix} \cos\alpha & 0 & -\sin\alpha \\ 0 & 1 & 0 \\ \sin\alpha & 0 & \cos\alpha \end{bmatrix}. \tag{7}$$

Therefore the varying parameter α affects all terms of the satellite dynamic model. To avoid computing models for each α value, the trick consists in isolating, through a feedback, a parameter that allows to generate all models during an appendage revolution, so does the LFR building step. But the cos and sin functions do not lend themselves to a LFR, since they are not rational expressions in α. Moreover these two functions are not independent: for all α values, the basic relationship

$$\cos^2\alpha + \sin^2\alpha = 1 \tag{8}$$

must be verified.

The choice of the parameter must be reviewed. Indeed rational expressions of the $\cos\alpha$ and $\sin\alpha$ functions can be derived in terms of a new varying parameter $\tau_1 = \tan(\frac{\alpha}{2})$ [1]:

$$\sin\alpha = \frac{2\tau_1}{1+\tau_1^2} \qquad \cos\alpha = \frac{1-\tau_1^2}{1+\tau_1^2} \tag{9}$$

But for a full revolution of the appendage ($\alpha \in [-\pi;\pi]$), τ_1 must vary from $-\infty$ to $+\infty$. This can be constraining, e.g. when a worst-case configuration is searched for with μ-analysis tools.

A better choice is the varying parameter $\tau_2 = \tan(\frac{\alpha}{4})$, as proposed in [18], because a complete revolution of the appendage is characterized by a τ_2 variation from -1 to 1:

$$\begin{aligned} \cos\alpha &= \frac{(1+\tau_2^2)^2 - 8\tau_2^2}{(1+\tau_2^2)^2} \qquad \forall \tau_2 \in]-1;1[\\ \sin\alpha &= \frac{4\tau_2(1-\tau_2^2)}{(1+\tau_2^2)^2} \qquad \forall \tau_2 \in]-1;1[\end{aligned} \tag{10}$$

Figure 8 shows that the block τ_2 can be repeated only four times to represent the first line of the matrix R_α. A block manipulation leads to a minimal LFR-type representation (see Fig. 6) where $\Delta = \tau_2 I_4$. A similar result can be found for the third line of R_α. Finally the LFR-type representation of the matrix R requires a minimal block $\Delta = \tau_2 I_{16}$.

It leads to a LFR-type representation of the whole satellite, which allows to analyze the closed-loop stability for a complete revolution of the appendage.

4 Illustration: closed-loop stability analysis

This section illustrates the advantages of the τ_2 parametrization to build the spacecraft model at a given angular configuration and to validate a control law on a full revolution of the appendage.

4.1 Study case

Let us consider a satellite composed of a main body and a flexible appendage connected to the main body through a rigid revolute joint along y_a-axis (locked at an arbitrary angular configuration by the appendage driven system). Flexibility is modelled by the four first flexible modes. Main body data and flexible appendage data are respectively summarized in Tab. 1 and 2. An appendage tilt around the y_a-axis is taken into account through the added matrix R_α defined in Eqn. (7).

4.2 Open-loop frequency-domain analysis

The inverse dynamic model of the overall spacecraft $\left[M^{\mathcal{B}+\mathcal{A}}_{G_{total}}(s)\right]^{-1}$ is computed using the block-diagram approach presented in section 2.

Figure 9 represents the BODE magnitude plots between the last 3 inputs and the last 3 outputs of $\left[M^{\mathcal{B}+\mathcal{A}}_{G_{total}}(s)\right]^{-1}$, when α is fixed at 0 deg. This restricted (3×3) transfer matrix is obviously symmetric. Plots are coherent with Tab. 2. Indeed antiresonances occur at frequencies of the 4 cantilevered flexible modes. Two of them are observable on the angular acceleration along x_b-axis (or x_a-axis, since $\alpha = 0$ deg) in accordance with the L_P definition, whereas only one contributes to the angular acceleration along z_b-axis (or z_a-axis). Moreover, as the coordinate axes of $\mathcal{R}_b$ are not the principal axes of the overall system, couplings between the 3 axes appear but they are low. That is why a synthesis axis per axis can be performed.

Figure 10 represents BODE magnitude plots of the transfer between external torque on x_b-axis at G_{total} and the absolute angular acceleration of $\mathcal{B}$ on x_b-axis, at different values of α. It illustrates how flexible modes evolve when the tilt angle of the appendage varies. A variation of steady-state gain can also be noted.

Same BODE magnitude plots are logically obtained at two configurations: $\alpha = 0$ deg and $\alpha = 180$ deg. Moreover the BODE magnitude plot obtained at $\alpha = 90$ deg corresponds exactly to the BODE magnitude plot of the transfer between external torque on z_b-axis at G_{total} and the absolute angular acceleration of $\mathcal{B}$ on z_b-axis (drawn in the lower right plot of Fig. 9): flexible mode resonances permute from x_b-axis to z_b-axis when α varies from 0 deg to 90 deg.

4.3 Proportional-Derivative controller synthesis

It is assumed that the 6 outputs of the model $H(s)$ (see Fig. 5) are measured.

Colocated rate sensors and torque actuators give rise to positive real transfer functions. It is well known that negative feedback with a strictly positive real controller ensures closed-loop stability. Moreover, as explained before, the 3 axes are almost decoupled. Consequently, the attitude control law is composed of 3 decoupled Proportional-Derivative controllers tuned on the total static inertia of the spacecraft.

Considering the x_b-axis, let J_x be:

$$J_x = M^{\mathcal{B}+\mathcal{A}}_{G_{total}}(0)\,(4,4) \tag{11}$$

then $K_{p_x} = \omega_{des}^2 J_x$ and $K_{v_x} = 2\xi_{des}\omega_{des} J_x$ where ω_{des} and ξ_{des} are respectively the required closed-loop bandwidth and damping ratio. The same approach is applied on the y_b and z_b-axes.

The resulting static control law is $u = Ky$ with

$$K = -\left[\text{diag}([\,K_{v_x}\ K_{v_y}\ K_{v_z}\,]) \quad \text{diag}([\,K_{p_x}\ K_{p_y}\ K_{p_z}\,])\right] \tag{12}$$

Further results are obtained with ξ_{des} and ω_{des} values respectively equal to 0.7 and $0.3\,rad\,s^{-1}$ for the 3 axes.

4.4 Closed-loop stability analysis

The next step consists in validating the closed-loop stability with the true flexible model $H(s)$

- when α varies from -180 deg to 180 deg,
- and in taking into account the transmission delays due to actuators dynamics.

The closed-loop system is depicted in Fig. 11. Time delays are approximated by second order PADE filters. Nominal values are $0.1\,s$ for the transfers along x_b and y_b-axes and $0.8\,s$ for the transfer along z_b-axis. Moreover such a stability analysis requires the α parametrization of the full flexible model. The methodology, explained in Sec. 3.2, leads to an LFR-type representation of the linear tilt-varying model, as depicted in Fig. 11. The tilt parameter τ_2 is repeated 16 times, since only rotational degrees of freedom are considered.

An EVANS root locus can be used to plot the evolution of the closed-loop poles in the complex plane when τ_2 varies from -1 to 1 (that is when α varies from -180 to 180 deg) and to analyse directly the closed-loop stability over a complete revolution of the appendage. Such a root locus is depicted in Fig.12 for the considered study case. Only the positive imaginary half-plane is represented. Note that due to the geometrical symmetry of the spacecraft, the root loci obtained when α varies from -180 to 0 deg and when α varies from 0 to 180 deg are identical. Fig. 12 directly shows that some angular configurations around $\alpha = +/-90$ deg are destabilized by the static controller K. Indeed, as positivity of the open-loop transfer is no more ensured due to transmision delays, closed-loop stability can no more be guaranteed. To counter these unstable configurations a lead phase controller must be tuned. The re-design of the controller is out of the scope of this paper but it can be recommended to use the worst-case angular configuration (that is $\alpha = 90$ deg) to tune the new controller.

5 Conclusions

This article has two main contributions, useful for satellite advanced design phase. First, it introduces a generic modeling approach for satellites with flexible appendages. This approach allows to take easily into account uncertainties on physical parameters and ensures to obtain a minimal realization of the overall system. Secondly, when tilted flexible appendages are considered, a new LFR-type representation is introduced to obtain a parametrization of the rotation angle of each appendage. Moreover, it is straightforward to deduce if a controller stabilizes the overall system for all angular configurations. It is no more required to compute the model of the whole satellite for each angular configuration. During verification and validation simulation steps, such a structured model could save lots of CPU-time.

References

[1] Cumer, C., and Chretien, J. P., 2001. "Minimal LFT form of a spacecraft built up from two bodies". In AIAA Guidance, Navigation, and Control Conference.

[2] Girard, A., and Roy, N., 2003. *Dynamics of Structure in Industry*. Lavoisier.

[3] Clough, R., and Penzien, J., 2003. *Dynamics of Structure*. Computers & Structures, Inc.

[4] Sidi, M., 1997. *Spacecraft Dynamics and Control : A practical Engineering Approach*. Cambridge University Press.

[5] Bodineau, G., Beugnon, C., Boulade, S., and Bérard-Chiappa, C., 2006. "μ-ITERATION Technique Applied to the Control of Satellites with Large Flexible Appendages". In Guidance, Navigation and Control Systems, Vol. 606 of *ESA Special Publication*.

[6] Craig, R. R., Chang, C. J., Aeronautics, U. S. N., Administration, S., Center, L. R., and of Texas at Austin, U., 1977. *Substructure coupling for dynamic analysis and testing*. No. vol. 2781 in NASA contractor report. National Aeronautics and Space Administration.

[7] Imbert, J., 1991. *Analyse des structures par éléments finis*. Cépaduès éd.

[8] Pascal, M., 1988. "Dynamics analysis of a system of hinge-connected flexible bodies". *Celestial Mechanics,* **41**, pp. 253–274.

[9] Alazard, D., Cumer, C., and Tantawi, K., 2008. "Linear dynamic modeling of spacecraft with various flexible appendages and on-board angular momentums". In ESA Guidance, Navigation, and Control Conference.

[10] Guy, N., Alazard, D., Cumer, C., and Charbonnel, C., 2011. "Modeling of satellite dynamics with uncertainties". In ESA Guidance, Navigation, and Control Conference.
[11] Lim, K. B., 1996. A robust control design framework for substructure models. Available at *http://ntrs.nasa.gov/archive/nasa/casi.ntrs.nasa.gov*.
[12] Maghami, P. G., and Lim, K. B., 2009. "Synthesis and Control of Flexible Systems With Component-Level Uncertainties". *Journal of dynamic systems, measurement, and control,* **131**.
[13] Boulet, B., Francis, B. A., Hughes, P., and Hong, T., 1997. "Uncertainty modeling and experiments in hscr; infin; control of large flexible space structure". *Control Systems Technology, IEEE Transactions on,* **5**(5), sep, pp. 504 –519.
[14] Ferreres, G., 1999. *A Practical Approach to Robustness Analysis with Aeronautical Applications*. Kluwer Academics/Plenum Press.
[15] Beck, C., and D'Andrea, R., 1998. "Computational study and comparisons of lft reducibility methods". In American Control Conference, 1998. Proceedings of the 1998, Vol. 2, pp. 1013–1017 vol.2.
[16] Varga, A., and Looye, G., 1999. "Symbolic and numerical software tools for lft-based low order uncertainty modeling". In In Proc. CACSD'99 Symposium, Cohala, pp. 1–6.
[17] Biannic, J.-M., and Döll, C. The LFRT toolbox. available at the web page *http://www.onera.fr/staff-en/jean-marc-biannic/*.
[18] Gaulocher, S., Chretien, J. P., Pittet, C., Delpech, M., and Alazard, D., 2004. "Closed-loop control of formation flying satellites: Time and parameter varying framework". In 2nd Int. Symposium on Formation Flying Missions and Technologies.
[19] Kumar, R., 2012. "Active vibration control of beams by combining precompressed layer damping and acld treatment: Performance comparison of various robust control techniques". *Journal of Vibration and Acoustics,* **134**(2).

Appendix A: Transport of a dynamic model from one point to another

This appendix summarizes the results presented in [9]. Let us consider a body $\mathcal{S}$, characterized by the 6 dof model:

$$\begin{bmatrix} \overrightarrow{F}_{/\mathcal{S}} \\ \overrightarrow{T}_{U/\mathcal{S}} \end{bmatrix} = D_U^{\mathcal{S}} \begin{bmatrix} \overrightarrow{a}_U \\ \overrightarrow{\omega} \end{bmatrix} \tag{13}$$

where U is any point, $\begin{bmatrix} \overrightarrow{F}_{/\mathcal{S}} \\ \overrightarrow{T}_{U/\mathcal{S}} \end{bmatrix}$ (resp. $\begin{bmatrix} \overrightarrow{a}_U \\ \overrightarrow{\omega} \end{bmatrix}$) is the 6 component vector of forces/torques applied to $\mathcal{S}$ at point U (resp. the 6 component vector of absolute linear and angular velocities of $\mathcal{S}$ at point U).

$D_U^{\mathcal{S}}$ is called the dynamic model matrix of $\mathcal{S}$ at point U and its expression depends on the frame where it is written. $D_U^{\mathcal{S}}$ is either a (6×6) static matrix (if $\mathcal{S}$ is a rigid body) or a (6×6) transfer matrix (if $\mathcal{S}$ is a flexible body).

The fisrt order approximation of dynamic model matrix of $\mathcal{S}$ at a new point V is easily deduced from $D_U^{\mathcal{S}}$ following:

$$D_V^{\mathcal{S}} = \tau_{UV}^T D_U^{\mathcal{S}} \tau_{UV} \tag{14}$$

where τ_{UV} is the kinematic model associated to points U and V:

$$\tau_{UV} = \begin{bmatrix} I_3 & (^*UV) \\ 0_{3\times 3} & I_3 \end{bmatrix} . \tag{15}$$

$(^*UV)$ is the skew-symmetric matrix associated to the vector $\overrightarrow{UV}$. If $[x\,y\,z]^T$ is the coordinate vector of $\overrightarrow{UV}$ in a frame $\mathcal{R}_{\mathcal{S}}$, the expression of $(^*UV)$ in $\mathcal{R}_{\mathcal{S}}$ is:

$$(^*UV) = \begin{bmatrix} 0 & -z & y \\ z & 0 & -x \\ -y & x & 0 \end{bmatrix} . \tag{16}$$

Proof:

$$\overrightarrow{T}_{V/\mathcal{S}} = \overrightarrow{T}_{U/\mathcal{S}} +^* (VU)\overrightarrow{F}_{/\mathcal{S}} . \tag{17}$$

$$\overrightarrow{a}_U = \overrightarrow{a}_V + {}^*(UV)\overrightarrow{\omega} + O({}^*\omega\overrightarrow{\omega}) \,. \tag{18}$$

Neglecting the (non-linear) second-order term $O({}^*\omega\overrightarrow{\omega})$, one can write:

$$\begin{bmatrix} \overrightarrow{F}_{/\mathcal{S}} \\ \overrightarrow{T}_{V/\mathcal{S}} \end{bmatrix} = \underbrace{\begin{bmatrix} I_3 & 0_{3\times 3} \\ ({}^*VU) & I_3 \end{bmatrix}}_{\tau_{UV}^T} \begin{bmatrix} \overrightarrow{F}_{/\mathcal{S}} \\ \overrightarrow{T}_{U/\mathcal{S}} \end{bmatrix} \tag{19}$$

$$= \tau_{UV}^T D_U^{\mathcal{S}} \begin{bmatrix} \overrightarrow{a}_U \\ \overrightarrow{\omega} \end{bmatrix} \tag{20}$$

$$= \tau_{UV}^T D_U^{\mathcal{S}} \underbrace{\begin{bmatrix} I_3 & ({}^*UV) \\ 0_{3\times 3} & I_3 \end{bmatrix}}_{\tau_{UV}} \begin{bmatrix} \overrightarrow{a}_V \\ \overrightarrow{\omega} \end{bmatrix} \tag{21}$$

$$= \underbrace{\tau_{UV}^T D_U^{\mathcal{S}} \tau_{UV}}_{D_V^{\mathcal{S}}} \begin{bmatrix} \overrightarrow{a}_V \\ \overrightarrow{\omega} \end{bmatrix} \,. \tag{22}$$

□

Illustration: Let us consider the mass/inertia matrix of the appendage $\mathcal{A}$ at its center of mass G:

$$D_G^{\mathcal{A}} = \begin{bmatrix} m^{\mathcal{A}} I_3 & 0_{3\times 3} \\ 0_{3\times 3} & \mathbb{I}_G^{\mathcal{A}} \end{bmatrix} \,, \tag{23}$$

the mass/inertia model matrix $D_P^{\mathcal{A}}$ of the appendage at point P presented in section 2.2 is:

$$D_P^{\mathcal{A}} = \tau_{GP}^T D_G^{\mathcal{A}} \tau_{GP} = \begin{bmatrix} m^{\mathcal{A}} I_3 & m^{\mathcal{A}}({}^*GP) \\ -m^{\mathcal{A}}({}^*GP) & \mathbb{I}_G^{\mathcal{A}} - m^{\mathcal{A}}({}^*GP)^2 \end{bmatrix} \,. \tag{24}$$

Appendix B: Illustration of a minimal LFT realization

Let us consider a second order transfer function:

$$F(s) = \frac{\omega^2}{s^2 + 2\xi\omega s + \omega^2} \,. \tag{25}$$

where the angular frequency ω is considered as uncertain: $\omega = \omega_0(1+\delta)$. ω_0 is the nominal value and δ is a multiplicative uncertainty.

In [19] authors consider independent uncertainties on ω and ω^2. But such assumption may bring some unrealistic parametric configurations. Figure 13 shows that the uncertainty δ appears only 2 times in a minimal LFR. According to the general formalism depicted in Figure 6, this LFR reads:

$$H(s) := \begin{bmatrix} \dot{x_1} \\ \dot{x_2} \\ z_1 \\ z_2 \\ y \end{bmatrix} = \begin{bmatrix} 0 & 1 & 0 & 0 & 0 \\ -\omega_0^2 & -2\xi\omega_0 & \omega_0 & 1 & \omega_0^2 \\ -\omega_0 & 0 & 0 & 0 & \omega_0 \\ -\omega_0^2 & -2\xi\omega_0 & \omega_0 & 0 & \omega_0^2 \\ 1 & 0 & 0 & 0 & 0 \end{bmatrix} \begin{bmatrix} x_1 \\ x_2 \\ w_1 \\ w_2 \\ u \end{bmatrix} \tag{26}$$

with $\Delta = \delta I_2$.

Today the available numerical tools (like the Robust Control toolbox or the LFR toolbox [17]) are not able to give directly this minimal result (both of them lead to a LFT model where the uncertainty on ω is repeated at least three times if

the system is defined from the transfer function (25)). This very simple academic example highlights that the best way to model an uncertain system is to build a block-diagram representation, as proposed in Fig. 3, where the uncertain dynamic parameters can be easily isolated and repeated a minimal number of times. Then, the Simulink/LFR object interface [17] can be used to compute directly the minimal LFR of the system.

List of Figures

List of Tables

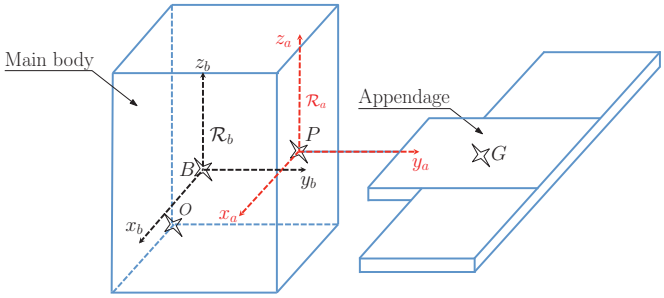

Fig. 1. Spacecraft composed of a main body and an appendage.

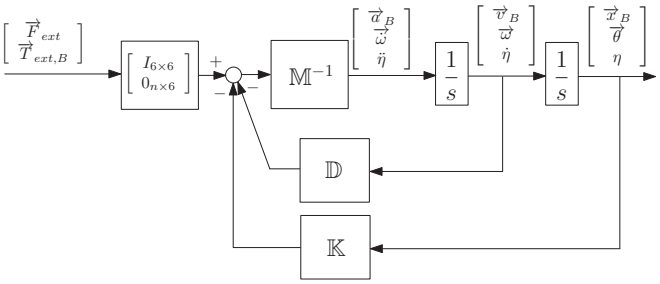

Fig. 2. "MDK" formulation.

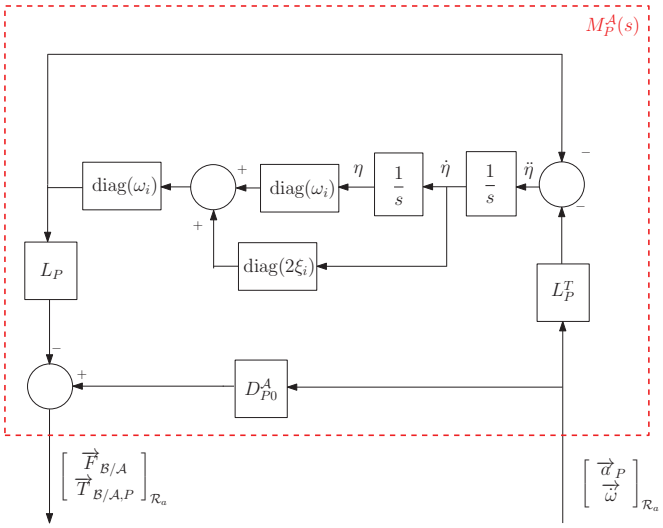

Fig. 3. Appendage dynamic model $M_P^{\mathcal{A}}(s)$: block-diagram representation based on the residual mass $D_{P,0}^{\mathcal{A}}$.

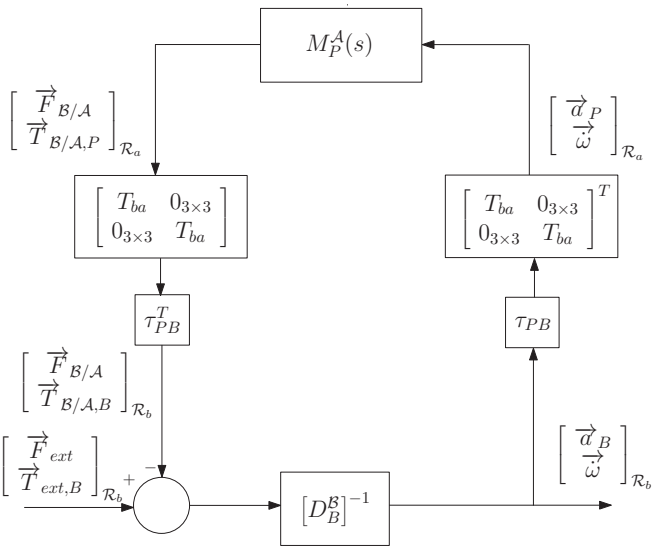

Fig. 4. Inverse dynamic model of the satellite $\left[M_B^{\mathcal{A}+\mathcal{B}}(s)\right]^{-1}$ at point B.

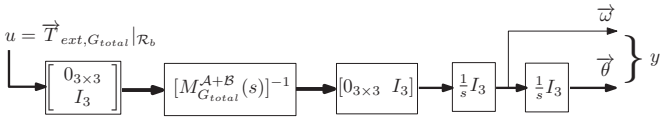

Fig. 5. The model $H(s)$ for attitude control.

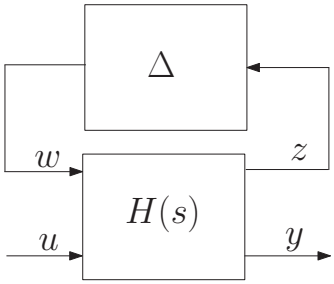

Fig. 6. A common LFR.

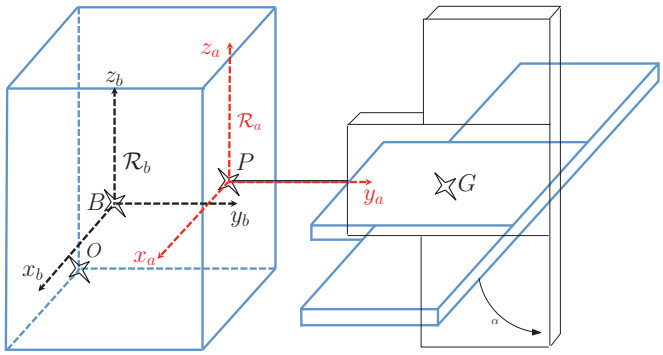

Fig. 7. Rotation of the appendage.

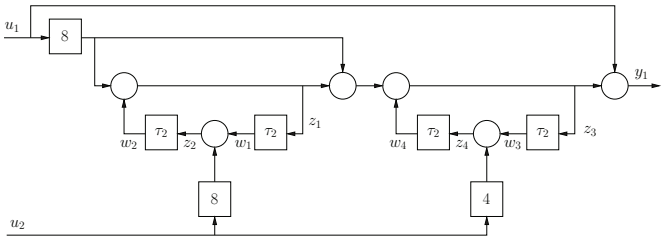

Fig. 8. Block-diagram representation of $y_1 = \cos\alpha\, u_1 - \sin\alpha\, u_2$ with a minimal occurrence of τ_2.

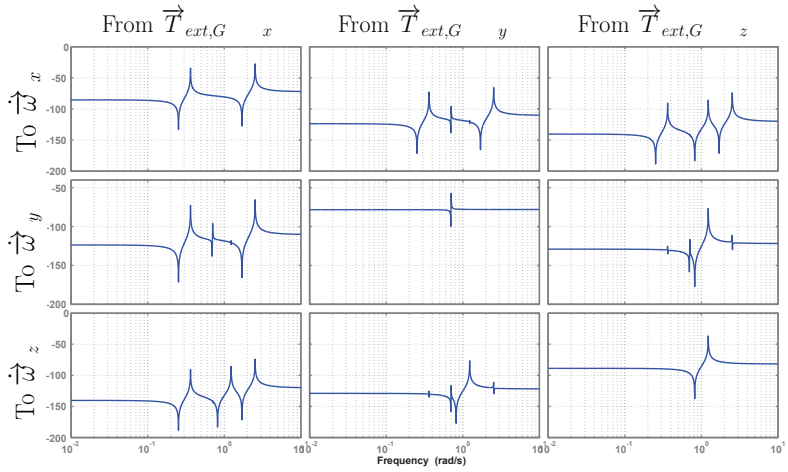

Fig. 9. BODE magnitude plot of the transfer between the 3 components of external torques (computed at G_{total} and written in $\mathcal{R}_b$) and the 3 components of the $\mathcal{B}$ absolute angular velocity, when $\alpha = 0$ deg.

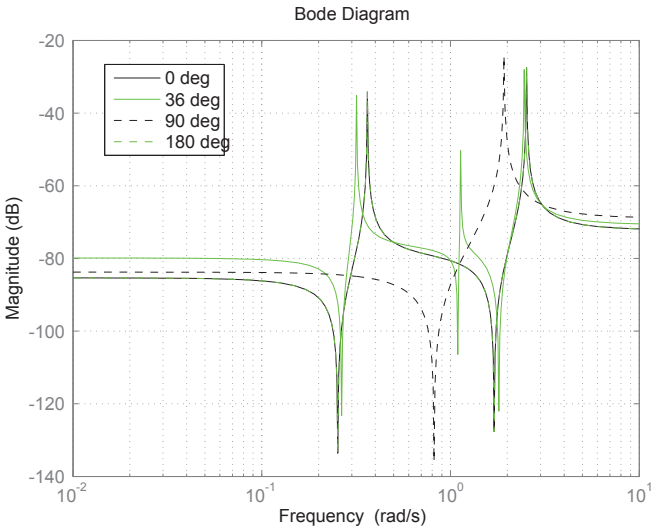

Fig. 10. BODE magnitude plot of the transfer between external torque on x_b-axis at G_{total} and absolute angular acceleration of $\mathcal{B}$ on x_b-axis for various title angle α.

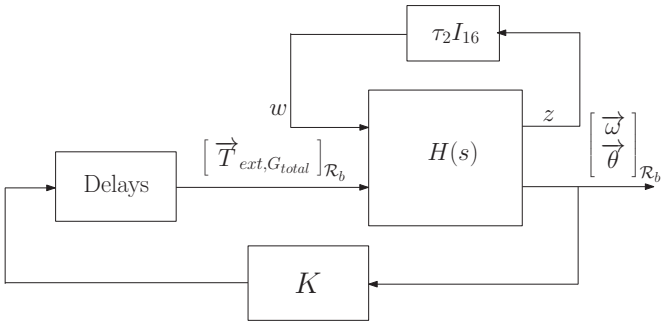

Fig. 11. Validation model of the controlled satellite.

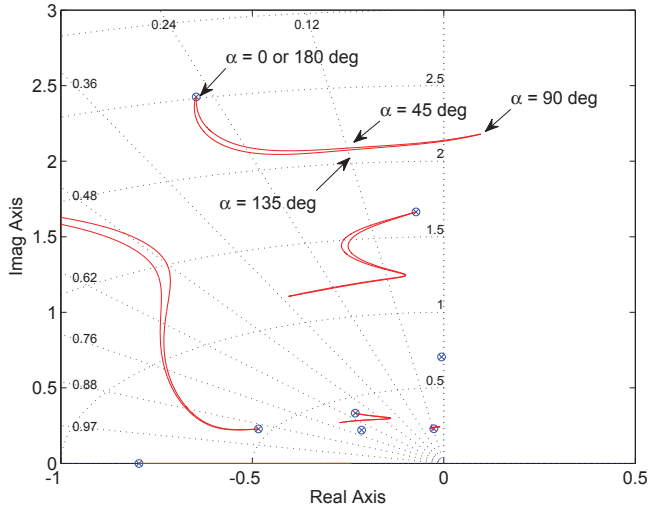

Fig. 12. Evolution of the poles of the closed-loop system, when α varies from 0 deg to 180 deg (i.e. $\tau_2 \in [0, 1]$).

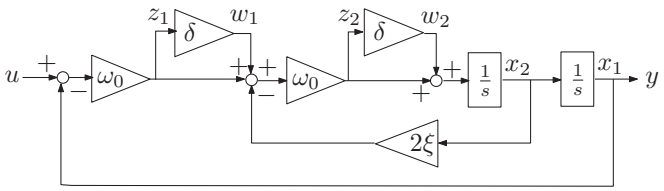

Fig. 13. Minimal LFR of system $F(s)$.

Main Body data	
$m^{\mathcal{B}}$: mass (kg)	2000
$\mathbb{I}_B^{\mathcal{B}}$: moment of inertia tensor w.r.t. B ($kg.m^2$) written in $\mathcal{R}_b$	$\begin{bmatrix} 2000 & 100 & 50 \\ 100 & 8000 & 80 \\ 50 & 80 & 8000 \end{bmatrix}$
$\overrightarrow{OB}$ written in $\mathcal{R}_o$ (m)	$\begin{bmatrix} 2 & 2 & 2 \end{bmatrix}^T$

Table 1. Definition of the main body.

Flexible appendage data	
$m^{\mathcal{A}}$: mass (kg)	100
$\overrightarrow{BP}$ written in $\mathcal{R}_b$ (m)	$\begin{bmatrix} 0 & 2 & 0 \end{bmatrix}^T$
$\mathbb{I}_G^{\mathcal{A}}$: moment of inertia tensor w.r.t. G written in $\mathcal{R}_a$ ($kg.m^2$)	$\begin{bmatrix} 7000 & 0 & 0 \\ 0 & 200 & 0 \\ 0 & 0 & 10000 \end{bmatrix}$
$\overrightarrow{PG}$ written in $\mathcal{R}_a$ (m)	$\begin{bmatrix} 0 & 8 & 0 \end{bmatrix}^T$
T_{ba}	I_3
ω_i: angular frequencies of the $N = 4$ cantilevered flexible modes ($rad\,s^{-1}$)	$2\pi * [\,0.04 \;\; 0.111 \;\; 0.13 \;\; 0.27\,]$
ξ_i: damping ratio of each flexible mode	0.001
L_P written in $\mathcal{R}_a$	$\begin{bmatrix} 0 & 0 & -3 & 0 \\ 0 & 0 & 0 & 0 \\ 5 & 0 & 0 & 4 \\ 90 & 0 & 0 & 62 \\ 0 & 14 & 0 & 0 \\ 0 & 0 & 119 & 0 \end{bmatrix}$

Table 2. Definition of the flexible appendage.